# We are IntechOpen,
# the world's leading publisher of
# Open Access books
# Built by scientists, for scientists

## 6,900
Open access books available

## 185,000
International authors and editors

## 200M
Downloads

## 154
Countries delivered to

Our authors are among the

## TOP 1%
most cited scientists

## 12.2%
Contributors from top 500 universities

**BOOK CITATION INDEX**
CLARIVATE ANALYTICS
INDEXED

**WEB OF SCIENCE™**

Selection of our books indexed in the Book Citation Index
in Web of Science™ Core Collection (BKCI)

# Interested in publishing with us?
# Contact book.department@intechopen.com

# Dynamic Analysis of a Spinning Laminated Composite-Material Shaft Using the *hp*- version of the Finite Element Method

Abdelkrim Boukhalfa
*Department of Mechanical Engineering, Faculty of Technology*
*University of Tlemcen*
*Algeria*

## 1. Introduction

Because of their high strength, high stiffness, and low density characteristics, composite materials are now used widely for the design of rotating mechanical components such as, for example, driveshafts for helicopters, cars and jet engines, or centrifugal separator cylindrical tubes. The interest of composites for rotordynamic applications has been demonstrated both numerically and experimentally. Accompanied by the development of many new advanced composite materials, various mathematical models of spinning composite shafts were also developed by researchers.

Zinberg and Symonds (Zinberg & Symonds, 1970) investigated the critical speeds for rotating anisotropic shafts and their experiments affirmed the advantages of composite shafts over aluminum alloy shafts. Using Donell's thin shell theory, Reis et al. (Dos Reis et al., 1987) applied finite element method to evaluate critical speeds of thin-walled laminated composite shafts. They concluded that the lay-up of a composite shaft strongly influences the dynamic behavior of this shaft.

Kim and Bert (Kim & Bert, 1993) utilized Sanders' best first approximation shell theory to determine critical speeds of a rotating shaft containing layers of arbitrarily laminated composite materials. Both the thin- and thick-shell models, including the Coriolis effect, were presented. Bert (Bert, 1992), as well as Bert and Kim (Bert & Kim, 1995a), examined critical speeds of composite shafts using Bernoulli-Euler beam theory and Bresse-Timoshenko beam model, respectively. Conventional beam model approaches used to date are Equivalent Modules Beam Theory (EMBT). In another study, Bert and Kim (Bert & Kim, 1995b) have analysed the dynamic instability of a composite drive shaft subjected to fluctuating torque and/or rotational speed by using various thin shell theories. The rotational effects include centrifugal and Coriolis forces. Dynamic instability regions for a long span simply supported shaft are presented.

M- Y. Chang et al (Chang et al., 2004a) published the vibration behaviours of the rotating composite shafts. In the model the transverse shear deformation, rotary inertia and gyroscopic effects, as well as the coupling effect due to the lamination of composite layers have been incorporated. The model based on a first order shear deformable beam theory

(continuum- based Timoshenko beam theory). M- Y. Chang et al (Chang et al., 2004b) published the vibration analysis of rotating composite shafts containing randomly oriented reinforcements. The Mori-Tanaka mean-field theory is adopted here to account for the interaction at the finite concentrations of reinforcements in the composite material.

Additional recent work on composite shafts dealing with both the theoretical and experimental aspects was reported by Singh (Singh, 1992), Gupta and Singh (Gupta & Singh, 1996) and Singh and Gupta (Singh & Gupta, 1994a). Rotordynamic formulation based on equivalent modulus beam theory was developed for a composite rotor with a number of lumped masses, and supported on general eight coefficient bearings. A Layerwise Beam Theory (LBT) was derived by Singh and Gupta (Gupta & Singh, 1996) from an available shell theory, with a layerwise displacement field, and was then extended to solve a general composite rotordynamic problem. The conventional rotor dynamic parameters as well as critical speeds, natural frequencies, damping factors, unbalance response and threshold of stability were analyzed in detail and results from the formulations based on the two theories, namely, the equivalent modulus beam theory (EMBT) and layerwise beam theory (LBT) were compared (Singh & Gupta, 1994a). The experimental rotordynamic studies carried by Singh and Gupta (Singh & Gupta, 1995-1996) were conducted on two filament wound carbon/epoxy shafts with constant winding angles (±45° and ±60°). Progressive balancing had to be carried out to enable the shaft to traverse through the first critical speed. Inspire of the very different shaft configurations used, the authors' have shown that bending-stretching coupling and shear-normal coupling effects change with stacking sequence, and alter the frequency values. Some practical aspects such as effect of shaft disk angular misalignment, interaction between shaft bow, which is common in composite shafts and rotor unbalance, and an unsuccessful operation of a composite rotor with an external damper were discussed and reported by Singh and Gupta (Singh & Gupta, 1995). The Bode and cascade plots were generated and orbital analysis at various operating speeds was performed. The experimental critical speeds showed good correlation with the theoretical prediction.

Mastering vibratory behavior requires knowledge of the characteristics of the composite material spinning shafts, the prediction of this knowledge is fundamental in the design of the rotating machinery in order to provide a precise idea of the safe intervals in terms of spinning speeds. Within the framework of this idea, our work concerns to the study of the vibratory behavior of the spinning composite material shafts, and more precisely, their behavior in rotation by taking into account the effects of the transverse shear deformation, rotary inertia and gyroscopic effects, as well as the coupling effect due to the lamination of composite layers, the effect of the elastic bearings and external damping and the effect of disk. In the presented composite shaft model, the Timoshenko theory will be adopted. An *hp-* version of the finite element method (combination between the conventional version of the finite element method (*h-* version) and the hierarchical finite element method (*p-* version) with trigonometric shape functions (Boukhalfa et al., 2008-2010) is used to model the structure. A hierarchical finite element of beam type with six degrees of freedom per node is developed. The assembly is made same manner as the standard version of the finite element method for several elements. The theoretical study allows the establishment of the kinetic energy and the strain energy of the system (shaft, disk and bearings) necessary to determine the motion equations. A program is elaborated to calculate the Eigen-frequencies and the critical speeds of the system. The results obtained are compared with those available in the literature and show the speed of convergence, the precision and the effectiveness of

Dynamic Analysis of a Spinning Laminated
Composite-Material Shaft Using the *hp*-version of the Finite Element Method
163

the method used. Several examples are treated, and a discussion is established to determine the influence of the various parameters and boundary conditions. In the *hp-* version of the finite element method, the error in the solution is controlled by both the number of elements *h* and the polynomial order *p* ((Babuska & Guo, 1986); (Demkowicz et al., 1989)). The *hp-*version of the finite element method has been exploited in a few areas including plate vibrations (Bardell et al., 1995) and beam statics (Bardell, 1996) and has been shown to offer considerable savings in computational effort when compared with the standard *h*-version of the finite element method.

## 2. Equations of motion

### 2.1 Kinetic and strain energy expressions of the shaft

The shaft is modeled as a Timoshenko beam, that is, first-order shear deformation theory with rotary inertia and gyroscopic effect is used. The shaft rotates at constant speed about its longitudinal axis. Due to the presence of fibers oriented than axially or circumferentially, coupling is made between bending and twisting. The shaft has a uniform, circular cross section.
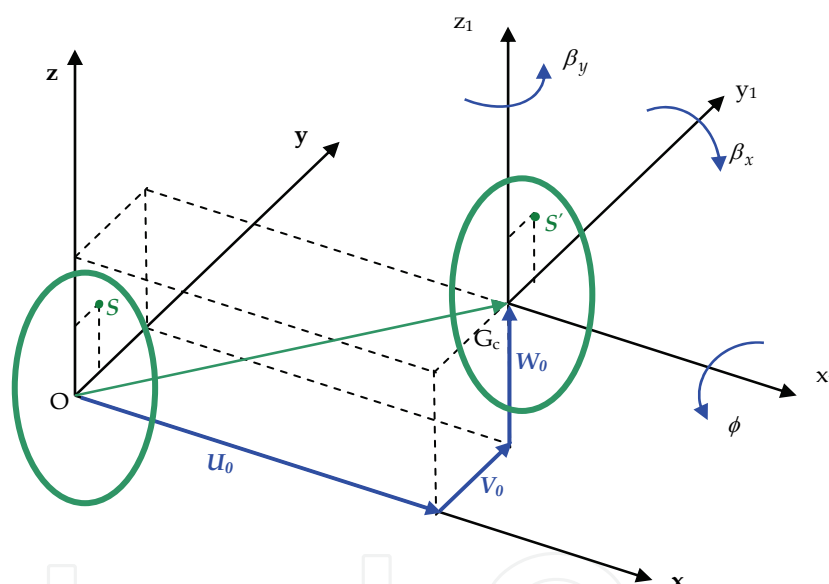


Fig. 1. The elastic displacements of a typical cross-section of the shaft

The following displacement field of a spinning shaft (one beam element) is assumed by choosing the coordinate axis *x* to coincide with the shaft axis:

$$\begin{cases} U(x,y,z,t) = U_0(x,t) + z\beta_x(x,t) - y\beta_y(x,t) \\ V(x,y,z,t) = V_0(x,t) - z\phi(x,t) \\ W(x,y,z,t) = W_0(x,t) + y\phi(x,t) \end{cases} \quad (1)$$

Where *U*, *V* and *W* are the flexural displacements of any point on the cross-section of the shaft in the *x*, *y* and *z* directions respectively, the variables $U_0$, $V_0$ and $W_0$ are the flexural displacements of the shaft's axis, while $\beta_x$ and $\beta_y$ are the rotation angles of the cross-section, about the *y* and *z* axis respectively. The $\phi$ is the angular displacement of the cross-section due to the torsion deformation of the shaft (see figure 1).

The strain components in the cylindrical coordinate system (As shown in figure 2-3) can be written in terms of the displacement variables defined earlier as

$$
\begin{cases}
\varepsilon_{xx} = \dfrac{\partial U_0}{\partial x} + r\sin\theta\dfrac{\partial \beta_x}{\partial x} - r\cos\theta\dfrac{\partial \beta_y}{\partial x} \\[2mm]
\varepsilon_{rr} = \varepsilon_{\theta\theta} = \varepsilon_{r\theta} = 0 \\[2mm]
\varepsilon_{x\theta} = \varepsilon_{\theta x} = \dfrac{1}{2}(\beta_y\sin\theta + \beta_x\cos\theta - \sin\theta\dfrac{\partial V_0}{\partial x} + \cos\theta\dfrac{\partial W_0}{\partial x} + r\dfrac{\partial \phi}{\partial x}) \\[2mm]
\varepsilon_{xr} = \varepsilon_{rx} = \dfrac{1}{2}(\beta_x\sin\theta - \beta_y\cos\theta - \sin\theta\dfrac{\partial W_0}{\partial x} + \cos\theta\dfrac{\partial V_0}{\partial x})
\end{cases}
\tag{2}
$$

Let us consider a composite shaft consists of $k$ layered (see figure 3) of fiber inclusion reinforced laminate. The constitutive relations for each layer are described by

$$
\begin{Bmatrix}
\sigma_{xx} \\
\sigma_{\theta\theta} \\
\sigma_{rr} \\
\tau_{r\theta} \\
\tau_{xr} \\
\tau_{x\theta}
\end{Bmatrix}
=
\begin{bmatrix}
C'_{11} & C'_{12} & C'_{13} & 0 & 0 & C'_{16} \\
C'_{12} & C'_{22} & C'_{23} & 0 & 0 & C'_{26} \\
C'_{13} & C'_{23} & C'_{33} & 0 & 0 & C'_{36} \\
0 & 0 & 0 & C'_{44} & C'_{45} & 0 \\
0 & 0 & 0 & C'_{45} & C'_{55} & 0 \\
C'_{16} & C'_{26} & C'_{36} & 0 & 0 & C'_{66}
\end{bmatrix}
\begin{Bmatrix}
\varepsilon_{xx} \\
\varepsilon_{\theta\theta} \\
\varepsilon_{rr} \\
\gamma_{r\theta} \\
\gamma_{xr} \\
\gamma_{x\theta}
\end{Bmatrix}
\tag{3}
$$

Where $C_{ij}'$ are the effective elastic constants, they are related to lamination angle $\eta$ (as shown in figure 4-5) and the elastic constants of principal axes.
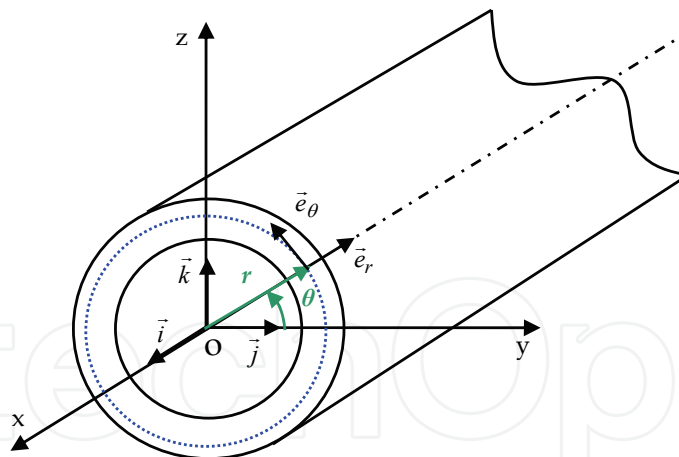


Fig. 2. The cylindrical coordinate System

The stress-strain relations of the $n$th layer expressed in the cylindrical coordinate system (see figure 6) can be expressed as

$$
\begin{cases}
\sigma_{xx} = C'_{11n}\varepsilon_{xx} + k_s C'_{16n}\gamma_{x\theta} \\[1mm]
\tau_{x\theta} = \tau_{\theta x} = k_s C'_{16n}\varepsilon_{xx} + k_s C'_{66n}\gamma_{x\theta} \\[1mm]
\tau_{xr} = \tau_{rx} = k_s C'_{55n}\gamma_{xr}
\end{cases}
\tag{4}
$$

Where $k_s$ is the transverse shear correction factor.
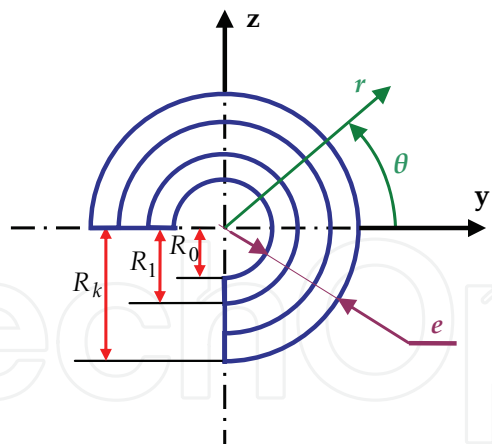
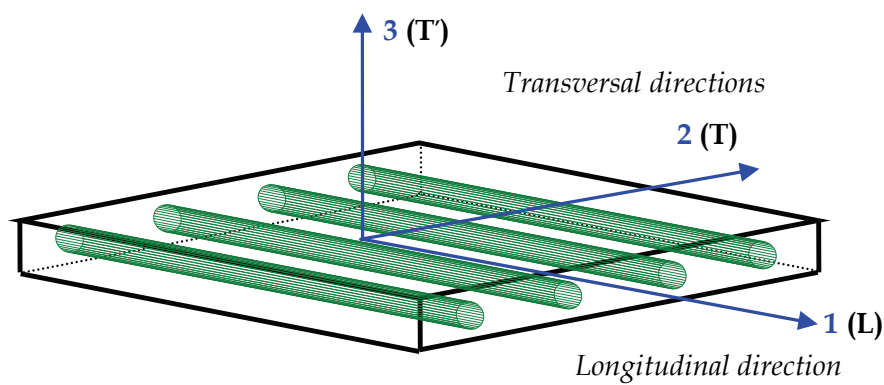Fig. 3. $k$ –layers of composite shaft



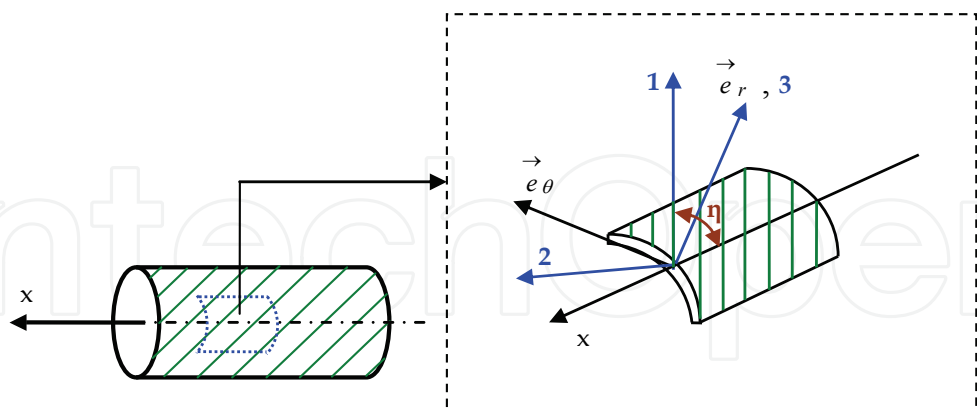Fig. 4. A typical composite lamina and its principal axes



Fig. 5. The definitions of the principal coordinate axes on an arbitrary layer of the composite

The formula of the strain energy is

$$E_d = \frac{1}{2}\int_V (\sigma_{xx}\varepsilon_{xx} + 2\tau_{xr}\varepsilon_{xr} + 2\tau_{x\theta}\varepsilon_{x\theta})\, dV \tag{5}$$

The various components of strain energy of the shaft are presented as follow (one beam element)

$$E_{da} = \frac{1}{2} A_{11} \int_0^L \left( \frac{\partial U_0}{\partial x} \right)^2 dx + \frac{1}{2} B_{11} \left[ \int_0^L \left( \frac{\partial \beta_x}{\partial x} \right)^2 dx + \int_0^L \left( \frac{\partial \beta_y}{\partial x} \right)^2 dx \right] + \frac{1}{2} k_s B_{66} \int_0^L \left( \frac{\partial \phi}{\partial x} \right)^2 dx +$$

$$\frac{1}{2} k_s A_{16} \left[ 2\int_0^L \frac{\partial \phi}{\partial x} \frac{\partial U_0}{\partial x} dx + \int_0^L \beta_y \frac{\partial \beta_x}{\partial x} dx - \int_0^L \beta_x \frac{\partial \beta_y}{\partial x} dx - \int_0^L \frac{\partial V_0}{\partial x} \frac{\partial \beta_x}{\partial x} dx - \int_0^L \frac{\partial W_0}{\partial x} \frac{\partial \beta_y}{\partial x} dx \right] + \quad (6)$$

$$\frac{1}{2} k_s (A_{55} + A_{66}) \left[ \int_0^L \left( \frac{\partial V_0}{\partial x} \right)^2 dx + \int_0^L \left( \frac{\partial W_0}{\partial x} \right)^2 dx + \int_0^L \beta_x^2 dx + \int_0^L \beta_y^2 dx + 2\int_0^L \beta_x \frac{\partial W_0}{\partial x} dx - 2\int_0^L \beta_y \frac{\partial V_0}{\partial x} dx \right]$$

where $A_{ij}$ and $B_{ij}$ are given in Appendix.

The kinetic energy of the spinning composite shaft (one beam element) (Boukhalfa et al., 2008), including the effects of translatory and rotary inertia, can be written as

$$E_{ca} = \frac{1}{2} \int_0^L \left[ I_m \left( \dot{U}_0{}^2 + \dot{V}_0{}^2 + \dot{W}_0{}^2 \right) + I_d \left( \dot{\beta}_x{}^2 + \dot{\beta}_y{}^2 \right) \right.$$

$$\left. -2\Omega I_p \beta_x \dot{\beta}_y + 2\Omega I_p \dot{\phi} + I_p \dot{\phi}^2 + \Omega^2 I_p + \Omega^2 I_d \left( \beta_x{}^2 + \beta_y{}^2 \right) \right] dx \quad (7)$$

where $\Omega$ is the rotating speed of the shaft which is assumed constant, $L$ is the length of the shaft, the $2\Omega I_p \beta_x \dot{\beta}_y$ term accounts for the gyroscopic effect, and $I_d \left( \dot{\beta}_x{}^2 + \dot{\beta}_y{}^2 \right)$ represent the rotary inertia effect. The mass moments of inertia $I_m$, the diametrical mass moments of inertia $I_d$ and polar mass moment of inertia $I_p$ of spinning shaft per unit length are defined in the appendix. As the $\Omega^2 I_d \left( \beta_x{}^2 + \beta_y{}^2 \right)$ term is far smaller than $\Omega^2 I_p$, it will be neglected in further analysis.
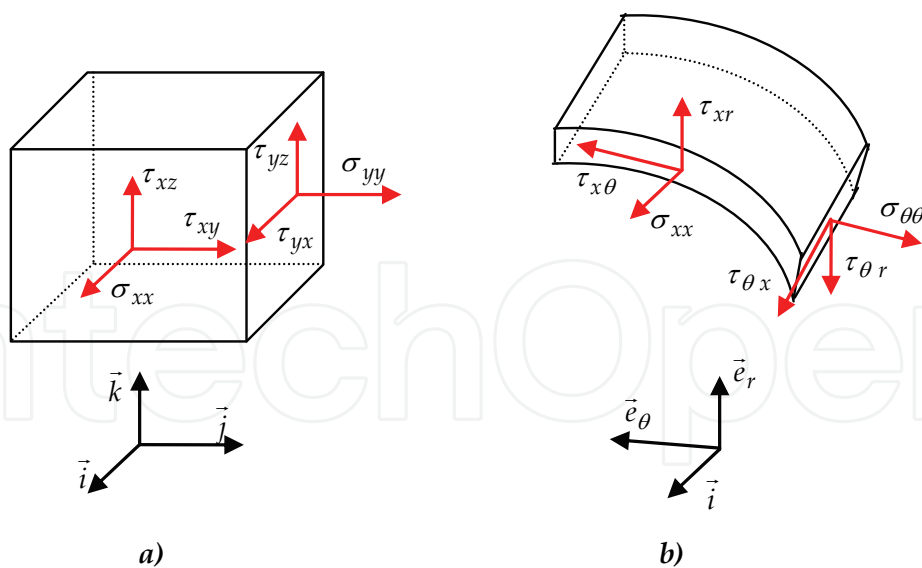


Fig. 6. The stress components; *a)* in the coordinate axes (*x, y, z*) - *b)* in the coordinate axes $(x, r, \theta)$

## 2.2 Kinetic energy of the disk

The disk fixed to the composite shaft (see figure 7) is assumed rigid and made of isotropic material. According to Equation (7) the kinetic energy of the disk can be expressed as

$$E_{cD} = \frac{1}{2}\Big[ I_m^D \Big(\dot{U}_0^2 + \dot{V}_0^2 + \dot{W}_0^2\Big) + I_d^D \Big(\dot{\beta}_x^2 + \dot{\beta}_y^2\Big)$$
$$-2\Omega I_p^D \beta_x \dot{\beta}_y + 2\Omega I_p^D \dot{\phi} + I_p^D \dot{\phi}^2 + \Omega^2 I_p^D + \Omega^2 I_d^D \Big(\beta_x^2 + \beta_y^2\Big)\Big]$$

(8)

where $I_m$, $I_d$ and $I_p$ are the mass, the diametrical mass moment of inertia and the polar mass moment of inertia of the disk. As the $\Omega^2 I_p^D \Big(\beta_x^2 + \beta_y^2\Big)$ term is far smaller than $\Omega^2 I_p^D$, it will be neglected in further analysis.
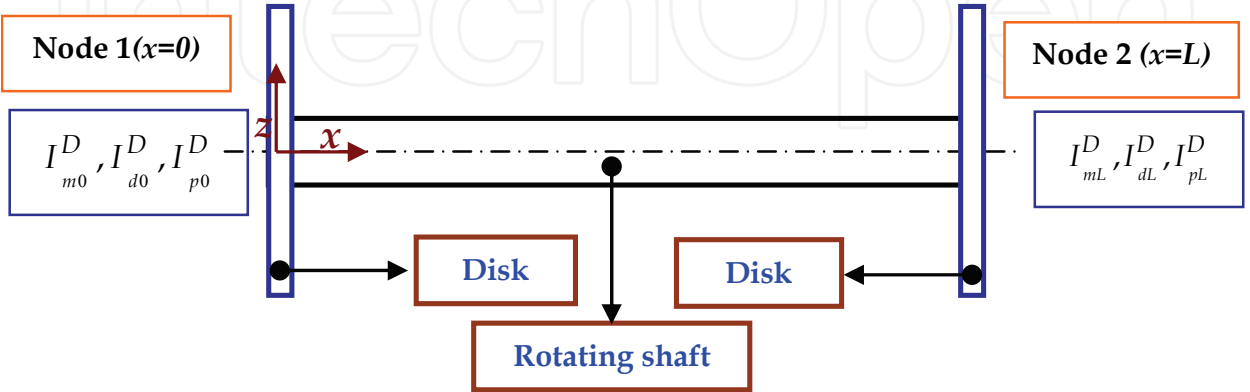


Fig. 7. Various positions of the disk on the spinning shaft (one element).

## 2.3 Virtual work of the bearings

The bearings are characterized by values of stiffness and viscous damping following the $y$ and $z$ directions and the cross terms (see Figures 8 and 9). The stiffness and damping effects of the bearings are modeled using springs and viscous dampers.
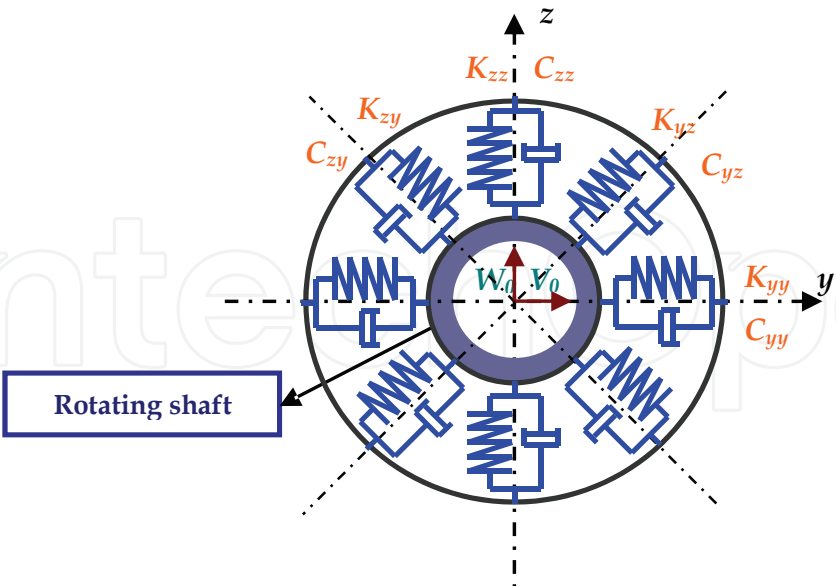


Fig. 8. Model of bearings

The virtual work $\delta A$ done by these external forces can be written as

$$\delta A = F_{V_0}\delta_{V_0} + F_{W_0}\delta_{W_0}$$

(9)

where $F_{V_0}$ and $F_{w_0}$ are the generalized forces expressed by

$$\begin{Bmatrix} F_{V0} \\ F_{W_0} \end{Bmatrix} = -\begin{bmatrix} C_{yy} & C_{yz} \\ C_{zy} & C_{zz} \end{bmatrix} \begin{Bmatrix} \dot{V}_0 \\ \dot{W}_0 \end{Bmatrix} - \begin{bmatrix} K_{yy} & K_{yz} \\ K_{zy} & K_{zz} \end{bmatrix} \begin{Bmatrix} V_0 \\ W_0 \end{Bmatrix} \tag{10}$$
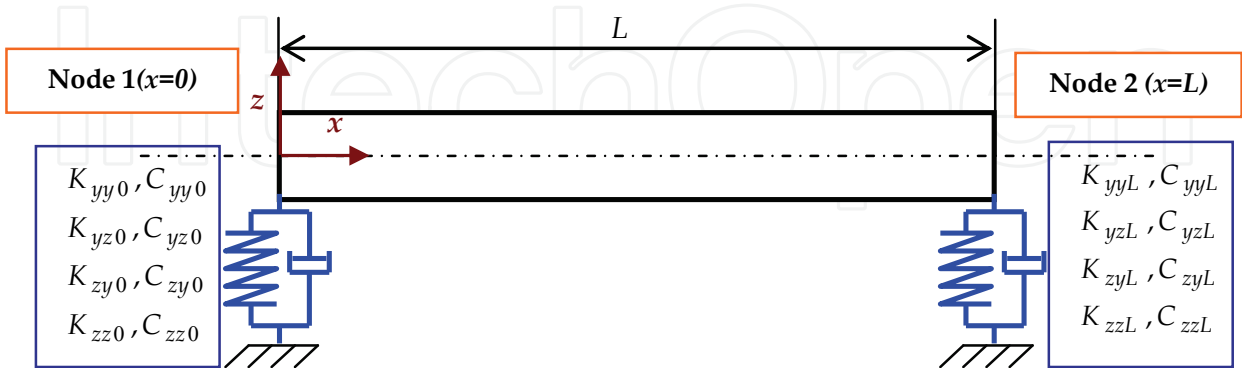


Fig. 9. Spinning shaft (one element) supported by two bearings

### 2.4 Hierarchical Beam element formulation

The spinning flexible beam is descretised by hierarchical beam elements. Each element with two nodes 1 and 2 is shown in figure 10. In the case of a staged shaft, several elements can be used (see figure 11). The element's nodal d.o.f. at each node are $U_0$, $V_0$, $W_0$, $\beta_x$, $\beta_y$ and $\phi$. The local and non-dimensional co-ordinates are related by

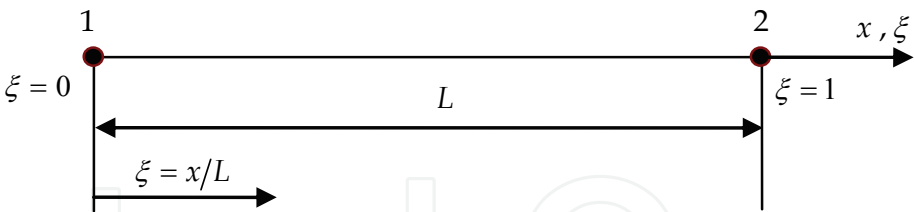$$\xi = x/L \qquad \text{With } (0 \le \xi \le 1) \tag{11}$$
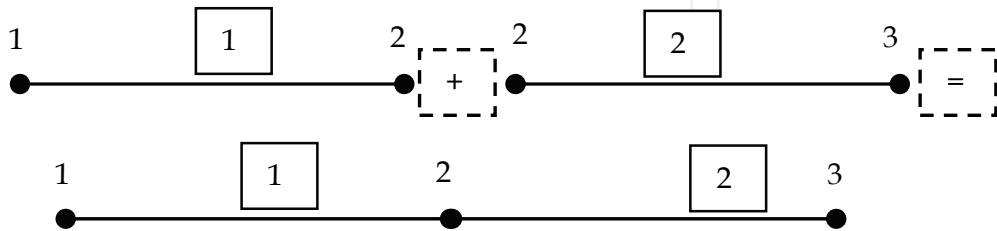


Fig. 10. 3D Beam element with two nodes



Fig. 11. Assembly between two $p$- elements

The vector displacement formed by the variables $U_0$, $V_0$, $W_0$, $\beta_x$, $\beta_y$ and $\phi$ can be written as

Dynamic Analysis of a Spinning Laminated
Composite-Material Shaft Using the *hp*-version of the Finite Element Method
169

$$
\left\{
\begin{aligned}
U_0 &= [N_U]\{q_U\} = \sum_{m=1}^{p_U} x_m(t) \cdot f_m(\xi) \\[2mm]
V_0 &= [N_V]\{q_V\} = \sum_{m=1}^{p_V} y_m(t) \cdot f_m(\xi) \\[2mm]
W_0 &= [N_W]\{q_W\} = \sum_{m=1}^{p_W} z_m(t) \cdot f_m(\xi) \\[2mm]
\beta_x &= \left[N_{\beta_x}\right]\{q_{\beta_x}\} = \sum_{m=1}^{p_{\beta_x}} \beta_{xm}(t) \cdot f_m(\xi) \\[2mm]
\beta_y &= \left[N_{\beta_y}\right]\{q_{\beta_y}\} = \sum_{m=1}^{p_{\beta_y}} \beta_{ym}(t) \cdot f_m(\xi) \\[2mm]
\phi &= \left[N_\phi\right]\{q_\phi\} = \sum_{m=1}^{p_\phi} \phi_m(t) \cdot f_m(\xi)
\end{aligned}
\right.
\tag{12}
$$

where [*N*] is the matrix of the shape functions, given by

$$
\left[ N_{U,V,W,\beta_x,\beta_y,\phi} \right] = \left[ f_1\, f_2 \ldots \ldots f_{p_U,p_V,p_W,p_{\beta_x},p_{\beta_y},p_\phi} \right]
\tag{13}
$$

where $p_U$, $p_V$, $p_W$, $p_{\beta_x}$, $p_{\beta_y}$ and $p_\phi$ are the numbers of hierarchical terms of displacements (are the numbers of shape functions of displacements). In this work, $p_U = p_V = p_W = p_{\beta_x} = p_{\beta_y} = p_\phi = p$
The vector of generalized coordinates given by

$$
\{q\} = \left\{ q_U, q_V, q_W, q_{\beta_x}, q_{\beta_y}, q_\phi \right\}^T
\tag{14}
$$

where

$$
\left\{
\begin{aligned}
&\{q_U\} = \left\{ x_1,x_2,x_3,\ldots,x_{p_U} \right\}^T \exp(j\omega t)\,;\, \{q_V\} = \left\{ y_1,y_2,y_3,\ldots,y_{p_V} \right\}^T \exp(j\omega t)\,; \\[2mm]
&\{q_W\} = \left\{ z_1,z_2,z_3,\ldots,y_{p_W} \right\}^T \exp(j\omega t)\,;\, \{q_{\beta_x}\} = \left\{ \beta_{x_1},\beta_{x_2},\beta_{x_3},\ldots,\beta_{x_{p_{\beta_x}}} \right\}^T \exp(j\omega t)\,; \\[2mm]
&\{q_{\beta_y}\} = \left\{ \beta_{y_1},\beta_{y_2},\beta_{y_3},\ldots,\beta_{y_{p_{\beta_y}}} \right\}^T \exp(j\omega t)\,;\, \{q_\phi\} = \left\{ \phi_1,\phi_2,\phi_3,\ldots,\phi_{p_\phi} \right\}^T \exp(j\omega t)
\end{aligned}
\right\}
\tag{15}
$$

The group of the shape functions used in this study is given by

$$
\left\{ (f_1 = 1-\xi)(f_2 = \xi)\left( f_{r+2} = \sin(\delta_r\,\xi), \delta_r = r\pi\,;\, r = 1,2,3,\ldots \right) \right\}
\tag{16}
$$

The functions ($f_1$, $f_2$) are those of the finite element method necessary to describe the nodal displacements of the element; whereas the trigonometric functions $f_{r+2}$ contribute only to the internal field of displacement and do not affect nodal displacements. The most attractive particularity of the trigonometric functions is that they offer great numerical stability. The shaft is modeled by elements called hierarchical finite elements with *p* shape functions for

each element. The assembly of these elements is done by the *h-* version of the finite element method.

After modelling the spinning composite shaft using the *hp-* version of the finite element method and applying the Euler-Lagrange equations, the motion's equations of free vibration of spinning flexible shaft can be obtained.

$$[M]\{\ddot{q}\} + \left[ [G] + \left[ C_p \right] \right] \{\dot{q}\} + [K]\{q\} = \{0\} \tag{17}$$

[*M*] and [*K*] are the mass and stiffness matrix respectively, [*G*] is the gyroscopic matrix and [*C_p*] is the damping matrix of the bearing (the different matrices of the equation (17) are given in the appendix).

## 3. Results

A program based on the formulation proposed to resolve the resolution of the equation (17).

### 3.1 Convergence

First, the mechanical properties of boron-epoxy are listed in table 1, and the geometric parameters are $L$ =2.47 m, $D$ =12.69 cm, $e$ =1.321 mm, 10 layers of equal thickness (90°, 45°,-45°,0°$_6$, 90°). The shear correction factor $k_s$ =0.503 and the rotating speed $\Omega$ =0. In this example, the boron -epoxy spinning shaft is modeled by one element of length $L$, then by two elements of equal length $L/2$.

|  | Graphite-epoxy | Boron-epoxy |
|---|---|---|
| $E_{11}$ (GPa) | 139.0 | 211.0 |
| $E_{22}$ (GPa) | 11.0 | 24.1 |
| $G_{12}$ (GPa) | 6.05 | 6.9 |
| $G_{23}$ (GPa) | 3.78 | 6.9 |
| $\nu_{12}$ | 0.313 | 0.36 |
| $\rho$ (kg/m³) | 1578.0 | 1967.0 |

Table 1. Properties of composite materials (Bert & Kim, 1995a)

The results of the five bending modes for various boundary conditions of the composite shaft as a function of the number of hierarchical terms $p$ are shown in figure 12. Figure clearly shows that rapid convergence from above to the exact values occurs when the number of hierarchical terms increased. The bending modes are the same for a number of hierarchical finite elements, equal 1 then 2. This shows the exactitude of the method even with one element and a reduced number of the shape functions. It is noticeable in the case of low frequencies, a very small $p$ is needed ($p$=4 sufficient), whereas in the case of the high frequencies, and in order to have a good convergence, $p$ should be increased.

### 3.2 Validation

In the following example, the critical speeds of composite shaft are analyzed and compared with those available in the literature to verify the present model. In this example, the composite hollow shafts made of boron-epoxy laminae, which are considered by Bert and

Dynamic Analysis of a Spinning Laminated
Composite-Material Shaft Using the *hp*-version of the Finite Element Method
171

Kim (Bert & Kim, 1995a), are investigated. The properties of material are listed in table1. The shaft has a total length of 2.47 m. The mean diameter D and the wall thickness of the shaft are 12.69 cm and 1.321 mm respectively. The lay-up is [90°/45°/-45°/0°$_6$/90°] starting from the inside surface of the hollow shaft. A shear correction factor of 0.503 is also used. The shaft is modeled by one element. The shaft is simply-supported at the ends. In this validation, *p* =10.
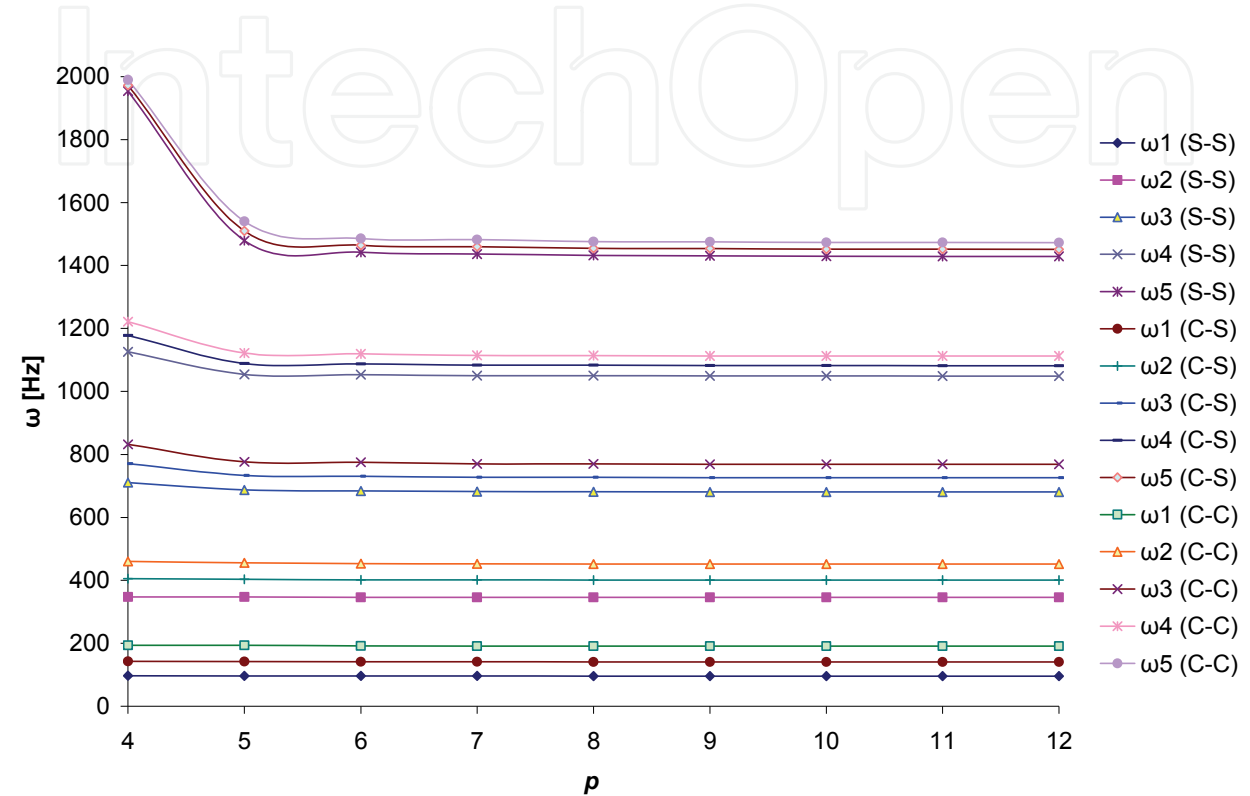


Fig. 12. Convergence of the frequency ω for the 5 bending modes of the composite shaft for different boundary conditions (S: simply-supported; C: clamped) as a function of the number of hierarchical terms *p*

The result obtained using the present model is shown in table 2 together with those of referenced papers. As can be seen from the table our results are close to those predicted by other beam theories. Since in the studied example the wall of the shaft is relatively thin, models based on shell theories (Kim & Bert, 1993) are expected to yield more accurate results. In the present example, the critical speed measured from the experiment however is still underestimated by using the Sander shell theory while overestimated by the Donnell shallow shell theory. In this case, the result from the present model is compatible to that of the Continuum based Timoshenko beam theory of M-Y. Chang et al (Chang et al., 2004a). In this reference the supports are flexible but in our application the supports are rigid.

In our work, the shaft is modeled by one element with two nodes, but in the model of the reference (Chang et al., 2004a) the shaft is modeled by 20 finite elements of equal length (*h*-version).  The rapid convergence while taking one element and a reduced number of shape functions shows the advantage of the method used. One should stress here that the present model is not only applicable to the thin-walled composite shafts as studied above, but also to the thick-walled shafts as well as to the solid ones.

| L=2.47 m, D =12.69 cm, e =1.321 mm, 10 layers of equal thickness  (90°, 45°,-45°,0°₆,90°) | | |
|---|---|---|
| | Theory or Method | $\Omega_{cr1}$ (rpm) |
| Zinberg & Symonds, 1970 | Measured experimentally<br>EMBT | 6000<br>5780 |
| Dos Reis et al., 1987 | Bernoulli–Euler beam theory with stiffness determined by shell finite elements | 4942 |
| Kim & Bert, 1993 | Sanders shell theory<br>Donnell shallow shell theory | 5872<br>6399 |
| Bert, 1992 | Bernoulli–Euler beam theory | 5919 |
| Bert & Kim, 1995a | Bresse–Timoshenko beam theory | 5788 |
| Singh & Gupta, 1996 | EMBT<br>LBT | 5747<br>5620 |
| Chang et al., 2004a | Continuum based Timoshenko beam theory | 5762 |
| Present | Timoshenko beam theory  by the *hp*- version of the FEM. | 5760 |

Table 2. The first critical speed of the boron-epoxy composite shaft

The first eigen-frequency of the boron-epoxy spinning shaft calculated by our program in the stationary case is 96.0594 Hz on rigid supports and 96.0575 Hz on two elastic supports of stiffness 1740 GN/m.  In the reference (Chatelet et al., 2002), they used the shell's theory for the same shaft studied in our case and on rigid supports; the frequency is 96 Hz.  In this example, is not noticeable the difference between shaft bi-supported on rigid supports or elastic supports because the stiffness of the supports are very large.

### 3.3 Results and interpretations
In this study, the results obtained for various applications are presented.  Convergence towards the exact solutions is studied by increasing the numbers of hierarchical shape functions for two elements.  The influence of the mechanical and geometrical parameters and the boundary conditions on the eigen-frequencies and the critical speeds of the embarked spinning composite shafts are studied. In this study, $p = 10$.

### 3.3.1 Influence of the gyroscopic effect on the eigen-frequencies
In the following example, the frequencies of a graphite- epoxy spinning shaft are analyzed. The mechanical properties of shaft are shown in table 1, with $k_s$ = 0.503.  The ply angles in the various layers and the geometrical properties are the same as those in the first example.
Figure 13 shows the variation of the bending fundamental frequency $\omega$ as a function of rotating speed $\Omega$ for different boundary conditions. The gyroscopic effect inherent to rotating structures induces a precession motion. When the rotating speed increase, the forward modes (1F) increase, whereas the backward modes (1B) decrease. The gyroscopic effect causes a coupling of orthogonal displacements to the axis of rotation, and by consequence separate the frequencies in two branches: backward precession mode and forward precession mode. In all cases, the forward modes increase with increasing rotating speed however the backward modes decrease.
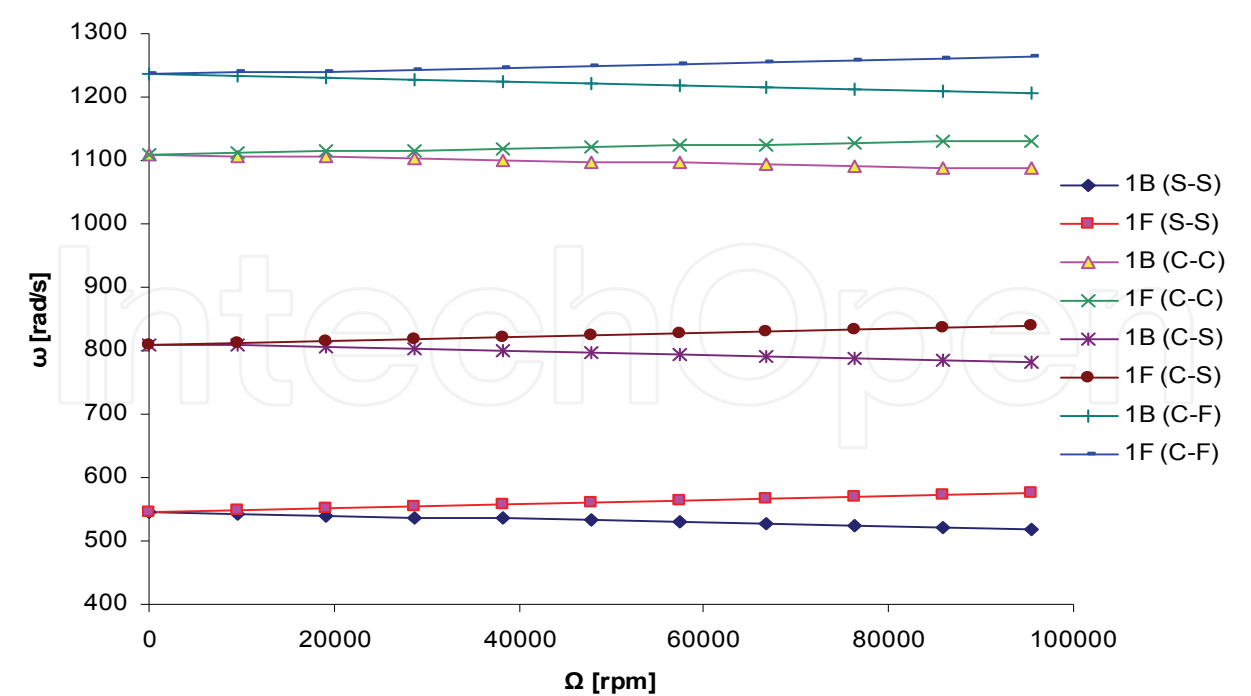
Fig. 13. The first backward (1B) and forward (1F) bending mode of a graphite- epoxy shaft
for different boundary conditions and different rotating speeds (S: simply-supported;
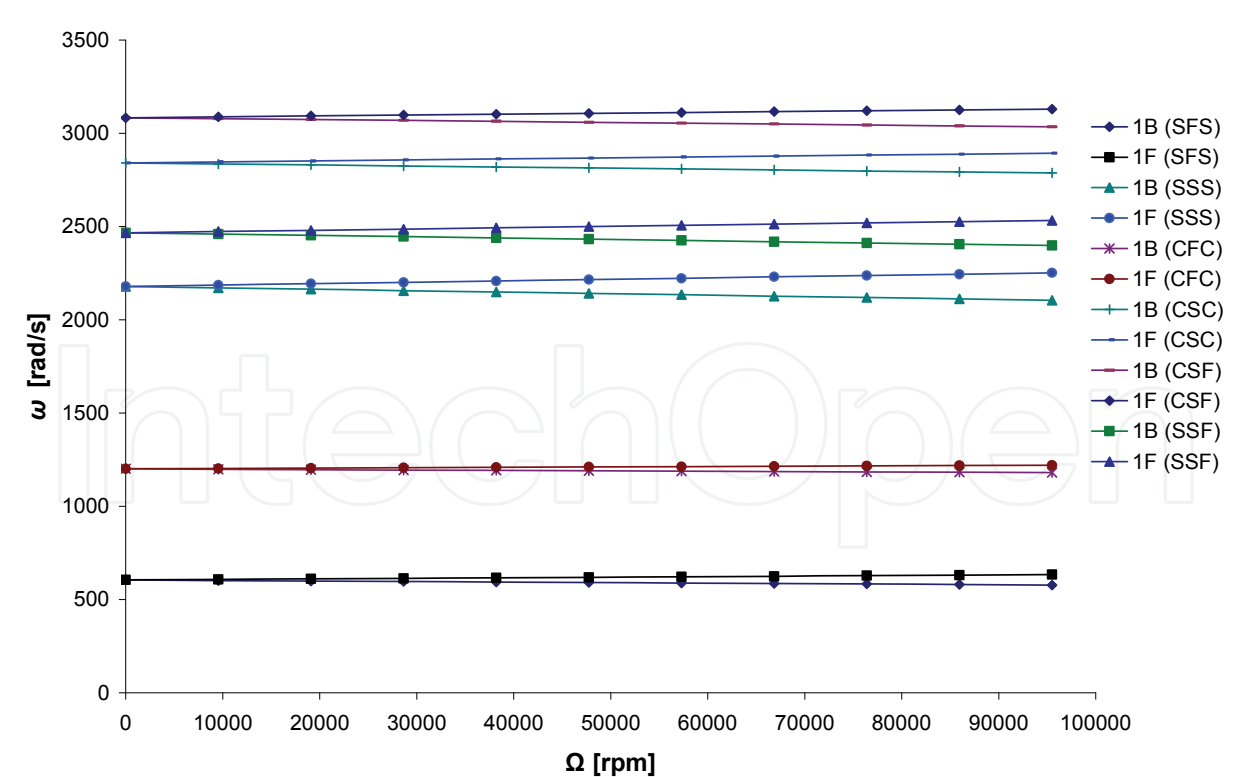C: clamped; F: free)



Fig. 14. The first backward (1B) and forward (1F) bending mode of a boron- epoxy shaft for
different boundary conditions and different rotating speeds. *L =2.47 m, D =12.69 cm, e =1.321
mm, 10 layers of equal thickness (90°, 45°,-45°,0°₆, 90°)*

### 3.3.2 Influence of the boundary conditions on the eigen-frequencies

In the following example, the boron-epoxy shaft is modeled by two elements of equal length $L/2$. The frequencies of the spinning shaft are analyzed. The mechanical properties of shaft are shown in table 1, with $k_s = 0.503$. The ply angles in the various layers and the geometrical properties are the same as those in the preceding example.

Figure 14 shows the variation of the bending fundamental frequency ω according to the rotating speeds $Ω$ for various boundary conditions. According to these found results, it is noticed that, the boundary conditions have a very significant influence on the eigen-frequencies of a spinning composite shaft. For example, by adding a support to the mid-span of the spinning shaft, the rigidity of the shaft increases which implies the increase in the eigen-frequencies.

### 3.3.3 Influence of the lamination angle on the eigen-frequencies

By considering the same preceding example, the lamination angles have been varied in order to see their influences on the eigen-frequencies of the spinning composite shaft.

Figure 15 shows the variation of the bending fundamental frequency ω according to the rotating speeds $Ω$ (Campbell diagram) for various ply angles. According to these results, the bending frequencies of the composite shaft decrease when the ply angle increases and vice versa.
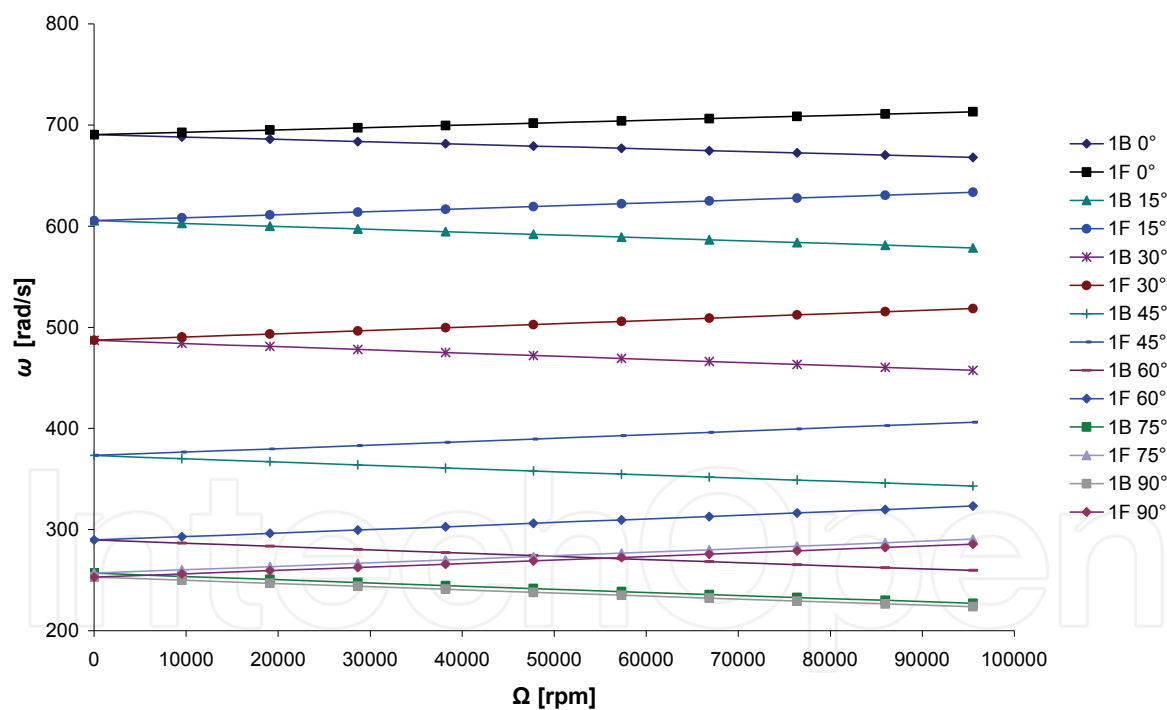


Fig. 15. The first backward (1B) and forward (1F) bending mode of a boron- epoxy shaft (S-S) for different lamination angles and different rotating speeds. *L =2.47 m, D =12.69 cm, e =1.321 mm, 10 layers of equal thickness*

### 3.3.4 Influence of the ratios L/D, e/D and η on the critical speeds and rigidity

The intersection point of the line $(Ω = ω)$ with the bending frequency curves (diagram of Campbell) indicate the speed at which the shaft will vibrate violently (i.e., the critical speed $Ω_{cr}$).

In figure 16, the first critical speeds of the graphite-epoxy composite shaft (the properties are listed in table 1, with $k_s$ =0.503) are plotted according to the lamination angle for various ratios *L/D* and various boundary conditions (S-S, C-C). From figure 16, the first critical speed of shaft bi-simply supported (S-S) has the maximum value at $\eta = 0°$ for a ratio *L/D* = 10, 15 and 20, and at $\eta = 15°$ for a ratio *L/D* = 5. For the case of a shaft bi-clamped (C-C), the maximum critical speed is at $\eta = 0°$ for a ratio *L/D* = 20 and at $\eta = 15°$ for a ratio *L/D* = 10 and 15, and at $\eta = 30°$ for a ratio *L/D* = 5.

Above results can be explained as follows. The bending rigidity reaches maximum at $\eta = 0°$ and reduces when the lamination angle increases; in addition, the shear rigidity reaches maximum at $\eta = 30°$ and minimum with $\eta = 0°$ and $\eta = 90°$. A situation in which the bending rigidity effect predominates causes the maximum to be $\eta = 0°$. However, as described by Singh ad Gupta (Singh & Gupta, 1994b), the maximum value shifts toward a higher lamination angle when the shear rigidity effect increases. Therefore, while comparing the phenomena of figure 16, the constraint from boundary conditions would raise the rigidity effect. A similar is observed for short shafts.
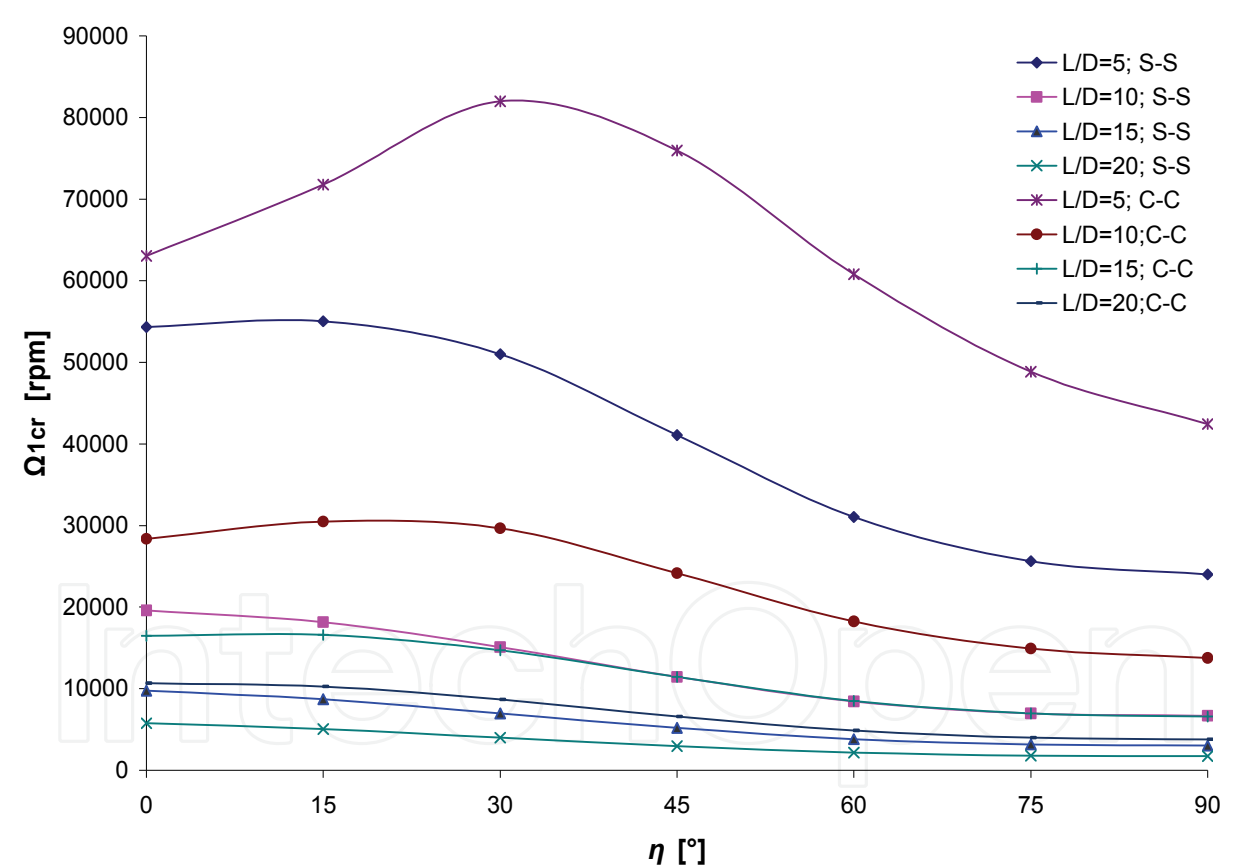


Fig. 16. The first critical speed $\Omega_{1cr}$ of spinning composite shaft according to the lamination angle $\eta$ for various ratios *L/D* and various boundary conditions (S-S, C-C)

In figures 17 and 18, the first critical speeds according to ratio *L/D* of the same graphite-epoxy shaft bi-simply supported (S-S) and the same graphite-epoxy shaft bi- clamped (C-C) for various lamination angles. It is noticeable, if ratio *L/D* increases, the critical speed decreases and vice versa.
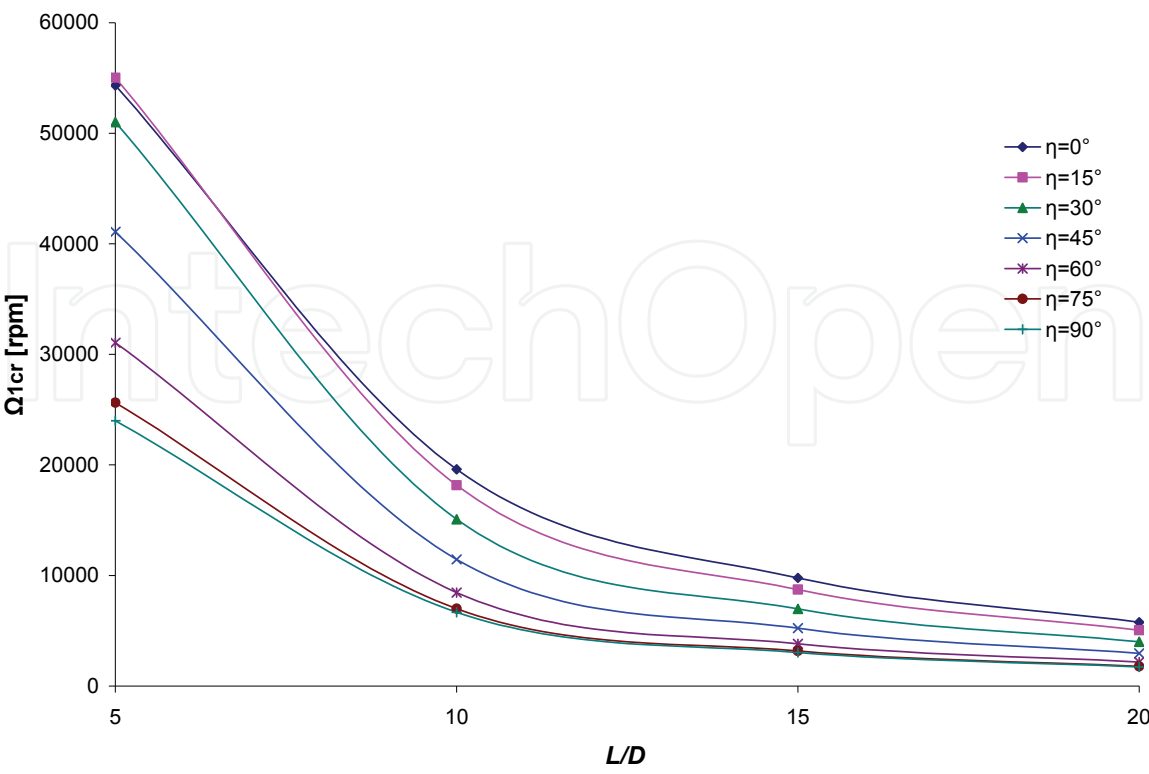
Fig. 17. The first critical speed $\Omega_{1cr}$ of spinning composite shaft bi- simply supported (S-S) according to ratio *L/D* for various lamination angles *η*
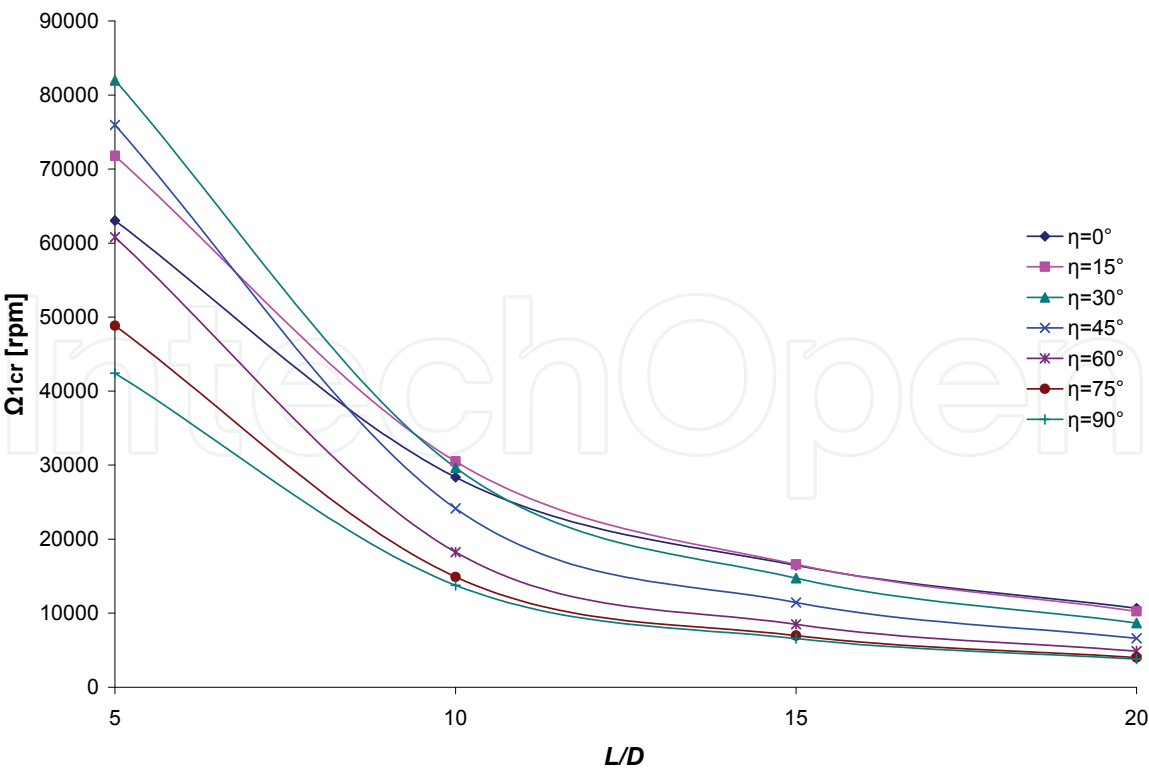


Fig. 18. The first critical speed $\Omega_{1cr}$ of spinning composite shaft bi- clamped (C-C) according to ratio *L/D* for various lamination angles *η*
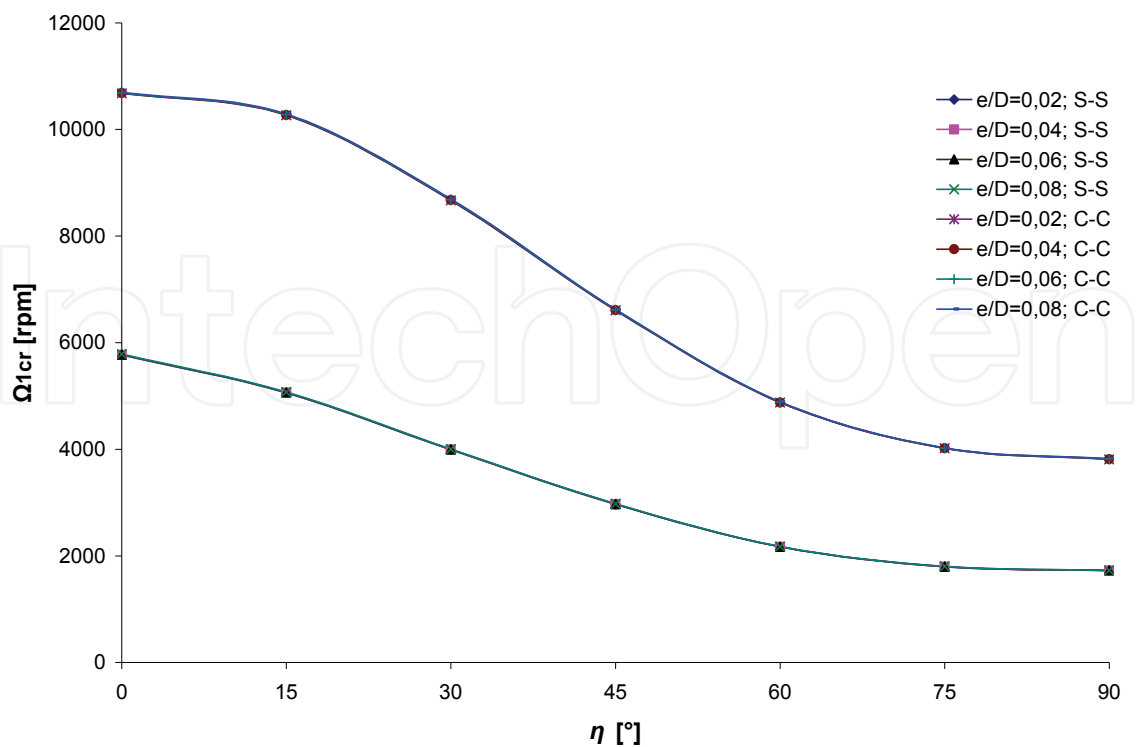
Fig. 19. The first critical speed $\Omega_{1cr}$ of spinning composite shaft according to the lamination angle $\eta$ for various ratios *e/D* and various boundary conditions (S-S, C-C); (*L/D* = 20)

Figure 19 plots the variation of first critical speeds of the same graphite-epoxy composite shaft with ratio *L/D* = 20 according to the lamination angle for various *e/D* ratios and various boundary conditions. It is noticed the influence of the *e/D* ratio on the critical speed is almost negligible; the curves are almost identical for the various *e/D* ratios of each boundary condition. This is due to the deformation of the cross section is negligible, and thus the critical speed of the thin-walled shaft would approximately independent of thickness ratio *e/D*. According to above results, while predicting which stacking sequence of the spinning composite shaft having the maximum critical speed, we should consider *L/D* ratio and the type of the boundary conditions. I.e., the maximum critical speed of a spinning composite shaft is not forever at ply angle equalizes zero degree, but it depends on the *L/D* ratio and the type the boundary conditions.

### 3.3.5 Influence of the stacking sequence on the eigen-frequencies

In order to show the effects of the stacking sequence on the eigen-frequencies, a spinning carbon- epoxy shaft is mounted on two rigid supports; the mechanical and geometrical properties of this shaft are (Singh & Gupta, 1996):

$E_{11}$ = 130 GPa, $E_{22}$ = 10 GPa, $G_{12} = G_{23}$ = 7 GPa, $v_{12}$ = 0.25, $\rho$ = 1500 Kg/m³

*L* =1.0 m, *D* = 0.1 m, *e* = 4 mm, 4 layers of equal thickness, $k_s$ = 0.503

A four-layered scheme was considered with two layers of 0° and two of 90° fibre angle. The flexural frequencies have been obtained for different combinations (both symmetric and unsymmetric) of 0° and 90° orientations (see figure 20). This figure plots the Campbell diagram of the first eigen-frequency of a spinning shaft for various stacking sequences. It can be observed from this figure that, for symmetric configurations, the frequency values of the spinning composite shaft are very close, and do have a slight dependence on the relative positioning of the 0° and 90° layers.
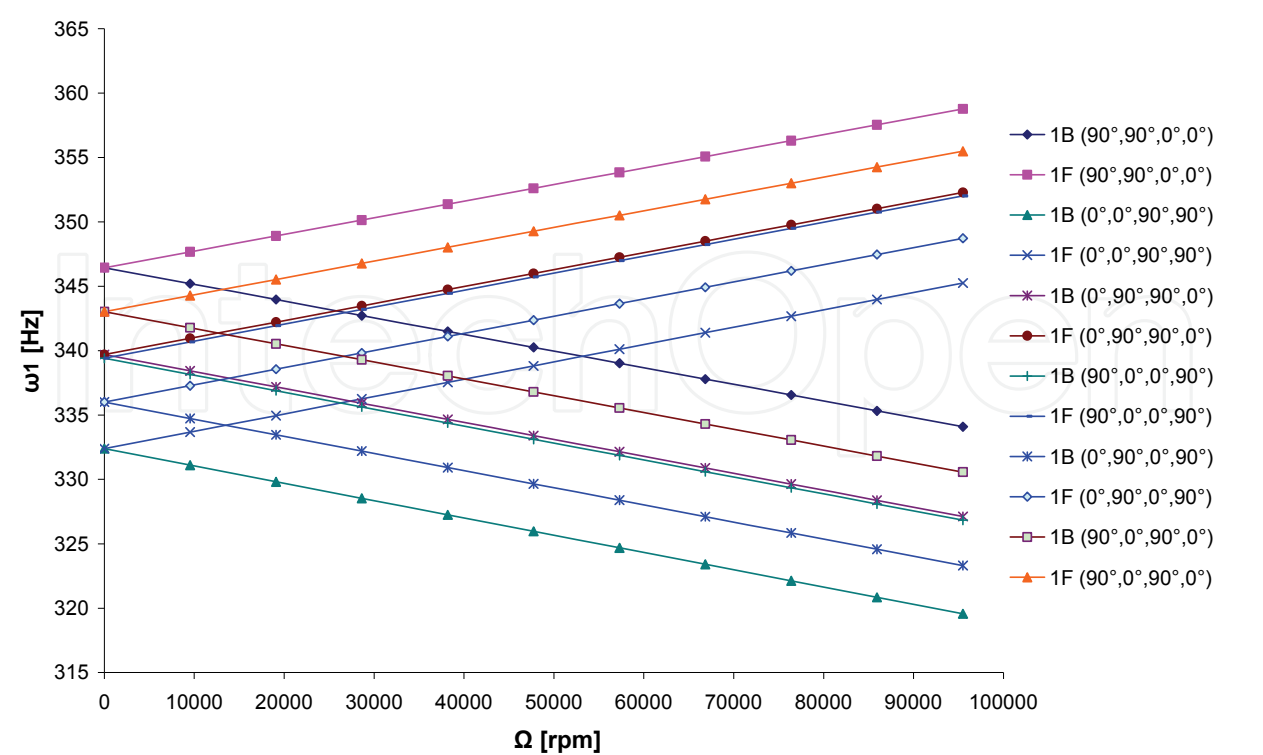
Fig. 20. First bending eigen-frequency of the spinning carbon- epoxy shaft bi- simply supported (S-S) for various stacking sequences according to the rotating speed

### 3.3.6 Influence of the disk's position according to the spinning shaft on on the eigen-frequencies

By considering another example, the eigen-frequencies of a graphite-epoxy shaft system are analyzed. The material properties are those listed in table 1. The lamination scheme remains the same as example 1, while its geometric properties, the properties of a uniform rigid disk are listed in table 3. The disk is placed at the mid-span of the shaft. The shaft system is shown in figure 21. For the finite element analysis, the shaft is modeled into two elements of equal lengths. The first element is simply-supported - free (S-F) and the second element is free- simply-supported (F-S). The disk is placed at the free boundary (F).
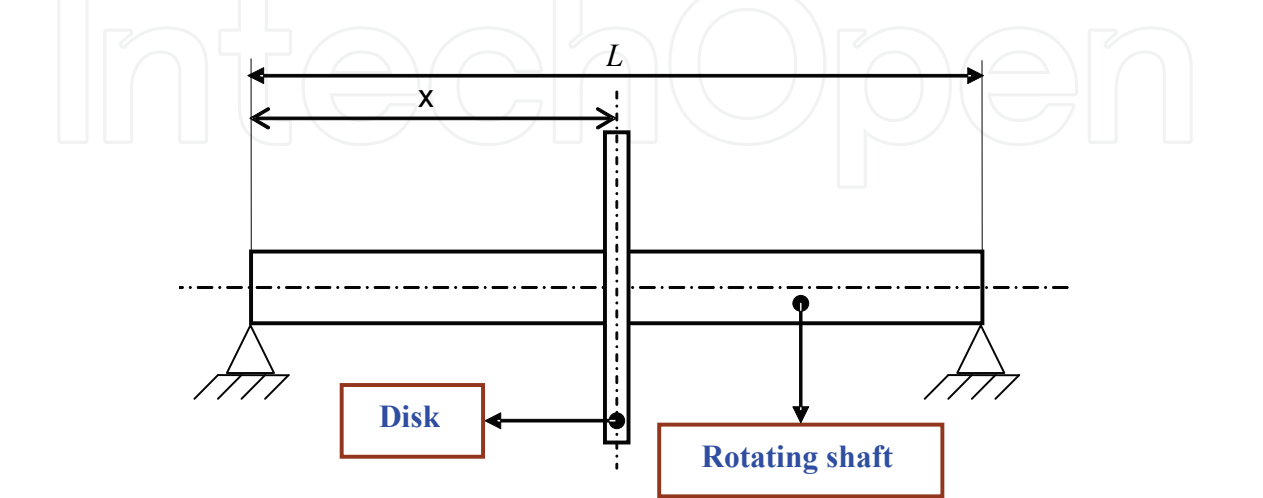


Fig. 21. System; embarked hollow spinning shaft.

The Campbell diagram containing the frequencies of the second pairs of bending whirling modes of the above composite system is shown in figure 22. Denote the ratio of the whirling bending frequency and the rotation speed of shaft as γ. The intersection point of the line (γ=1) with the whirling frequency curves indicate the speed at which the shaft will vibrate violently (i.e., the critical speed). In figure 22 the second pair of the forward and backward whirling frequencies falls more wide apart in contrast to other pairs of whirling modes. This might be due to the coupling of the pitching motion of the disk with the transverse vibration of shaft. Note that the disk is located at the mid-span of the shaft, while the second whirling forward and backward bending modes are skew-symmetric with respect to the mid-span of the shaft. Figure 23 shows the Campbell diagram of the first two bending frequencies of the embarked graphite- epoxy shaft for various disk's positions (x) according to the shaft (see figure 21). It is noted that when the disk approaches the support, the first bending frequency decreases and the second bending frequency increases and vice versa.

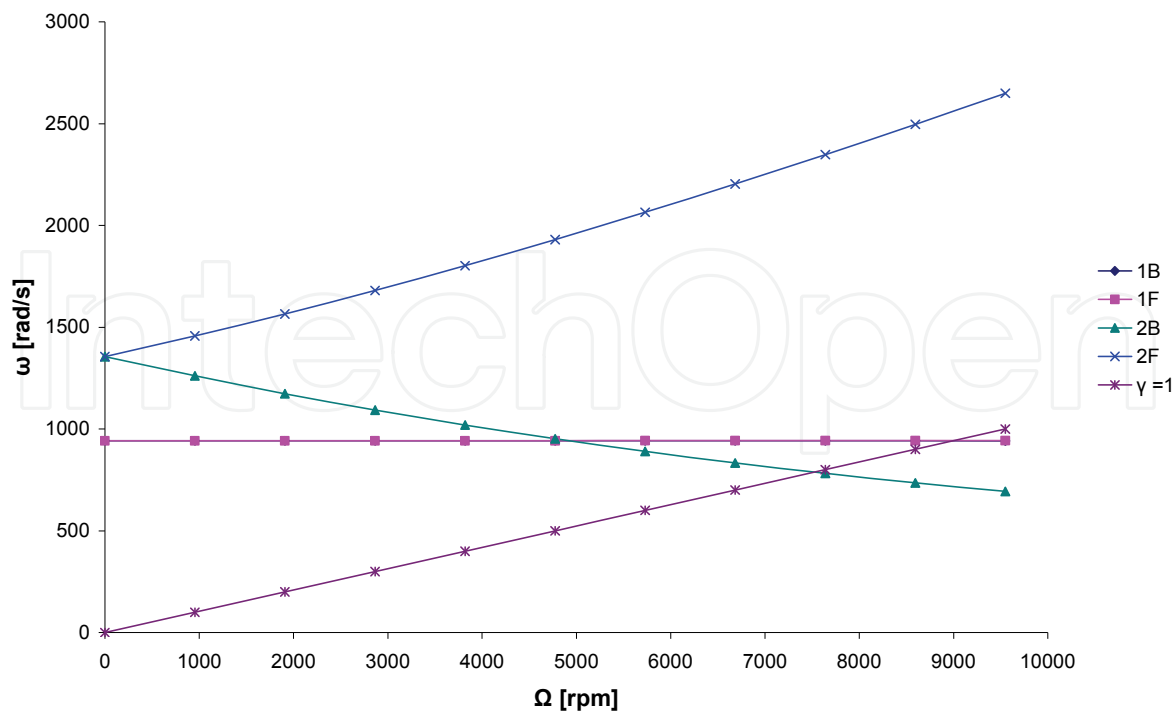| Properties | Shaft | Disk |
|---|---|---|
| L (m) | 0.72 | |
| Interior ray (m) | 0.028 | |
| external ray (m) | 0.048 | |
| $k_s$ | 0.56 | |
| $I_m$ (kg) | | 2.4364 |
| $I_d$ (kg m²) | | 0.1901 |
| $I_p$ (kg m²) | | 0.3778 |

Table 3. Properties of the system (shaft + disk)



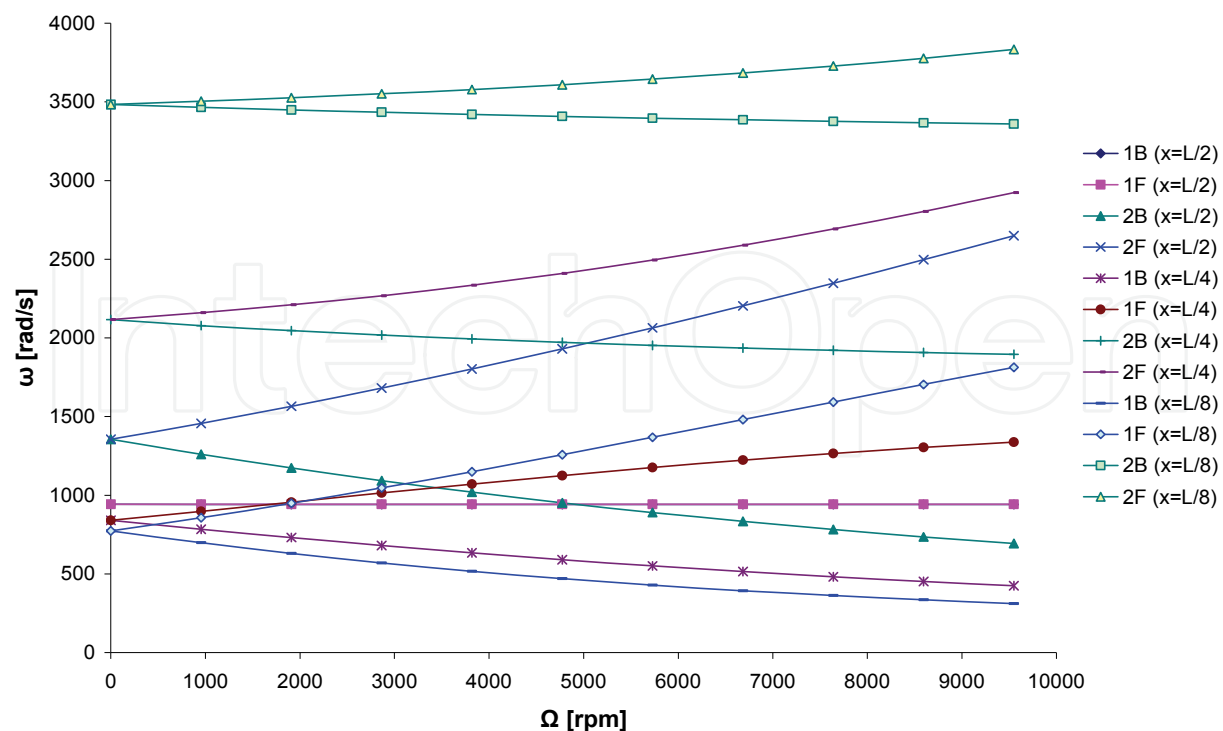Fig. 22. Campbell diagram of the first two bending frequencies of the embarked graphite-epoxy shaft

Fig. 23. Campbell diagram of the first two bending frequencies of the graphite-epoxy shaft for various disk's positions (x) according to the shaft

## 4. Conclusion

The analysis of the free vibrations of the spinning composite shafts using the *hp*-version of the finite element method (hierarchical finite element method (*p*-version) with trigonometric shape functions combined with the standard finite element method (*h*-version)), is presented in this work. The results obtained agree with those available in the literature. Several examples were treated to determine the influence of the various geometrical and physical parameters of the embarked spinning shafts. This work enabled us to arrive at the following conclusions:

a.  Monotonous and uniform convergence is checked by increasing the number of the shape functions *p*, and the number of the hierarchical finite elements *h*. The convergence of the solutions is ensured by the element beam with two nodes. The results agree with the solutions found in the literature.

b.  The gyroscopic effect causes a coupling of orthogonal displacements to the axis of rotation, and by consequence separates the frequencies in two branches, backward and forward precession modes. In all cases the forward modes increase with increasing rotating speed however the backward modes decrease. This effect has a significant influence on the behaviours of the spinning shafts.

c.  The dynamic characteristics and in particular the eigen-frequencies, the critical speeds and the bending and shear rigidity of the spinning composite shafts are influenced appreciably by changing the ply angle, the stacking sequence, the length, the mean diameter, the materials, the rotating speed and the boundary conditions.

d.  The critical speed of the thin-walled spinning composite shaft is approximately independent of the thickness ratio and mean diameter of the spinning shaft.

e.  The dynamic characteristics of the system (shaft + disk + support) are influenced appreciably by changing disk's positions according to the shaft.

Dynamic Analysis of a Spinning Laminated
Composite-Material Shaft Using the *hp*-version of the Finite Element Method
181

Prospects for future studies can be undertaken following this work: a study which takes into account damping interns in the case of a functionally graded material rotor with flexible disks, supported by supports with oil and subjected to disturbing forces like the air pockets or seisms, etc.

## 5. Nomenclature

| | |
|---|---|
| $U(x, y, z)$ | Displacement in x direction. |
| $V(x, y, z)$ | Displacement in y direction. |
| $W(x, y, z)$ | Displacement in z direction. |
| $\beta_x$ | Rotation angles of the cross-section about the y axis. |
| $\beta_y$ | Rotation angles of the cross-section, about the z axis. |
| $\phi$ | Angular displacement of the cross-section due to the torsion deformation of the shaft. |
| E | Young modulus. |
| G | Shear modulus. |
| (1, 2, 3) | Principal axes of a layer of laminate |
| (x, y, z) | Cartesian coordinates. |
| $(x, r, \theta)$ | Cylindrical coordinates. |
| $G_c$ | Centre of the cross-section. |
| (O, x, y, z) | Inertial reference frame. |
| $(G_c, x_1, y_1, z_1)$ | Local reference frame is located in the centre of the cross-section. |
| $C_{ij}'$ | Elastic constants. |
| $k_s$ | Shear correction factor. |
| v | Poisson coefficient. |
| $\rho$ | Masse density. |
| L | Length of the shaft. |
| D | Mean radius of the shaft. |
| e | Wall thickness of the shaft. |
| $R_n$ | The nth layer inner radius of the composite shaft. |
| $R_{n+1}$ | The nth layer outer radius of the composite shaft. |
| k | Number of the layer of the composite shaft. |
| $\eta$ | Lamination (ply) angle. |
| $\theta$ | Circumferential coordinate. |
| $\xi$ | Local and non-dimensional co-ordinates. |
| $\omega$ | Frequency, eigen-value. |
| $\Omega$ | Rotating speed. |
| [N] | Matrix of the shape functions. |
| $f(\xi)$ | Shape functions. |
| p | Number of the shape functions or number of hierarchical terms. |
| t | Time. |
| $E_c$ | Kinetic energy. |
| $E_d$ | Strain energy. |
| $\{q_i\}$ | Generalized coordinates, with (i = U, V, W, $\beta_x$, $\beta_y$, $\phi$) |
| [M] | Masse matrix. |
| [K] | Stiffness matrix. |
| [G] | Gyroscopic matrix. |

$[C_P]$                          Damping matrix.

$K_{yy0}, K_{yz0}, K_{zy0}, K_{zz0}$          Bearing stiffness coefficients in x = 0.

$K_{yyL}, K_{yzL}, K_{zyL}, K_{zzL}$          Bearing stiffness coefficients in x = L.

$C_{yy0}, C_{yz0}, C_{zy0}, C_{zz0}$          Bearing damping coefficients in x = 0.

$C_{yyL}, C_{yzL}, C_{zyL}, C_{zzL}$          Bearing damping coefficients in x = L.

## 6. Appendix

The terms $A_{ij}$, $B_{ij}$ of the equation (6) and $I_m$, $I_d$, $I_p$ of the equation (7) are given as follows:

$$
\begin{cases}
A_{11} = \pi \sum_{n=0}^{k} C'_{11n}(R_{n+1}^2 - R_n^2) \; ; \; A_{55} = \dfrac{\pi}{2} \sum_{n=0}^{k} C'_{55n}(R_{n+1}^2 - R_n^2) \\[2mm]
A_{66} = \dfrac{\pi}{2} \sum_{n=0}^{k} C'_{66n}(R_{n+1}^2 - R_n^2) \; ; \; A_{16} = \dfrac{2\pi}{3} \sum_{n=0}^{k} C'_{16n}(R_{n+1}^3 - R_n^3) \; ; \\[2mm]
B_{11} = \dfrac{\pi}{4} \sum_{n=0}^{k} C'_{11n}(R_{n+1}^4 - R_n^4) \; ; \; B_{66} = \dfrac{\pi}{2} \sum_{n=0}^{k} C'_{66n}(R_{n+1}^4 - R_n^4)
\end{cases}
\quad
\begin{cases}
I_m = \pi \sum_{n=0}^{k} \rho_n \left( R_{n+1}^2 - R_n^2 \right) \\[2mm]
I_d = \dfrac{\pi}{4} \sum_{n=0}^{k} \rho_n \left( R_{n+1}^4 - R_n^4 \right) \\[2mm]
I_p = \dfrac{\pi}{2} \sum_{n=0}^{k} \rho_n \left( R_{n+1}^4 - R_n^4 \right)
\end{cases}
\quad \text{A1-2}
$$

where $k$ is the number of the layer, $R_{n-1}$ is the $n$th layer inner radius of the composite shaft and $R_n$ it is the $n$th layer outer of the composite shaft. $L$ is the length of the composite shaft and $\rho_n$ is the density of the $n$th layer of the composite shaft.

The indices used in the matrix forms are as follows:

**a**: shaft; **D**: disk; **e**: element; **P**: bearing (support)

The various matrices of the equation (13) which assemble the elementary matrices of the system as follows

*- Shaft*

$$
\left[ M_a^e \right] =
\begin{bmatrix}
[M_U] & 0 & 0 & 0 & 0 & 0 \\
0 & [M_V] & 0 & 0 & 0 & 0 \\
0 & 0 & [M_W] & 0 & 0 & 0 \\
0 & 0 & 0 & [M_{\beta_x}] & 0 & 0 \\
0 & 0 & 0 & 0 & [M_{\beta_y}] & 0 \\
0 & 0 & 0 & 0 & 0 & [M_\phi]
\end{bmatrix}
\qquad \text{A3}
$$

$$
\left[ K_a^e \right] =
\begin{bmatrix}
[K_U] & 0 & 0 & 0 & 0 & [K_1] \\
0 & [K_V] & 0 & [K_2] & [K_3] & 0 \\
0 & 0 & [K_W] & [K_4] & [K_5] & 0 \\
0 & [K_2]^T & [K_4]^T & [K_{\beta_x}] & [K_6] & 0 \\
0 & [K_3]^T & [K_5]^T & [K_6]^T & [K_{\beta_y}] & 0 \\
[K_1]^T & 0 & 0 & 0 & 0 & [K_\phi]
\end{bmatrix}
\qquad \text{A4}
$$

Dynamic Analysis of a Spinning Laminated
Composite-Material Shaft Using the *hp*-version of the Finite Element Method
183

$$\left[ G_a^e \right] = \begin{bmatrix} 0 & 0 & 0 & 0 & 0 & 0 \\ 0 & 0 & 0 & 0 & 0 & 0 \\ 0 & 0 & 0 & 0 & 0 & 0 \\ 0 & 0 & 0 & 0 & [G_1] & 0 \\ 0 & 0 & 0 & -[G_1]^T & 0 & 0 \\ 0 & 0 & 0 & 0 & 0 & 0 \end{bmatrix} \qquad \text{A5}$$

$$[M_U] = I_m L \int_0^1 [N_U]^T [N_U]\, d\xi \;, \qquad [M_V] = I_m L \int_0^1 [N_V]^T [N_V]\, d\xi \qquad \text{A6-7}$$

$$[M_W] = I_m L \int_0^1 [N_W]^T [N_W]\, d\xi \;, \qquad \left[ M_{\beta_x} \right] = I_d L \int_0^1 \left[ N_{\beta_x} \right]^T \left[ N_{\beta_x} \right] d\xi \qquad \text{A8-9}$$

$$\left[ M_{\beta_y} \right] = I_d L \int_0^1 \left[ N_{\beta_y} \right]^T \left[ N_{\beta_y} \right] d\xi \;, \qquad \left[ M_\phi \right] = I_p L \int_0^1 \left[ N_\phi \right]^T \left[ N_\phi \right] d\xi \qquad \text{A10-11}$$

$$[K_U] = \frac{1}{L} A_{11} \int_0^1 [N_U']^T [N_U']\, d\xi \;, \qquad [K_V] = \frac{1}{L} k_s (A_{55} + A_{66}) \int_0^1 [N_V']^T [N_V']\, d\xi \qquad \text{A12-13}$$

$$[K_W] = \frac{1}{L} k_s (A_{55} + A_{66}) \int_0^1 [N_W']^T [N_W']\, d\xi \;, \quad [K_1] = \frac{1}{L} k_s A_{16} \int_0^1 \left[ N_\phi' \right]^T [N_U']\, d\xi \qquad \text{A14-15}$$

$$[K_2] = -\frac{1}{2L} k_s A_{16} \int_0^1 [N_V']^T \left[ N_{\beta_x}' \right] d\xi \;, \quad [K_3] = -k_s (A_{55} + A_{66}) \int_0^1 \left[ N_{\beta_y} \right]^T [N_V']\, d\xi \qquad \text{A16-17}$$

$$[K_4] = k_s (A_{55} + A_{66}) \int_0^1 \left[ N_{\beta_x} \right]^T [N_W']\, d\xi \;, \quad [K_5] = -\frac{1}{2L} k_s A_{16} \int_0^1 [N_W']^T \left[ N_{\beta_y}' \right] d\xi \qquad \text{A18-19}$$

$$[K_6] = \left[ \frac{1}{2} k_s A_{16} \int_0^1 \left[ N_{\beta_y} \right]^T \left[ N_{\beta_x}' \right] d\xi \right] - \left[ \frac{1}{2} k_s A_{16} \int_0^1 \left[ N_{\beta_x} \right]^T \left[ N_{\beta_y}' \right] d\xi \right] \qquad \text{A20}$$

$$\left[ K_{\beta_x} \right] = \left[ \frac{1}{L} B_{11} \int_0^1 \left[ N_{\beta_x}' \right]^T \left[ N_{\beta_x}' \right] d\xi \right] + \left[ L k_s (A_{55} + A_{66}) \int_0^1 \left[ N_{\beta_x} \right]^T \left[ N_{\beta_x} \right] d\xi \right] \qquad \text{A21}$$

$$\left[ K_{\beta_y} \right] = \left[ \frac{1}{L} B_{11} \int_0^1 \left[ N_{\beta_y}' \right]^T \left[ N_{\beta_y}' \right] d\xi \right] + \left[ L k_s (A_{55} + A_{66}) \int_0^1 \left[ N_{\beta_y} \right]^T \left[ N_{\beta_y} \right] d\xi \right] \qquad \text{A22}$$

$$\left[ K_\phi \right] = \frac{1}{L} B_{66} \int_0^1 \left[ N'_\phi \right]^T \left[ N'_\phi \right] d\xi \ , \ \left[ G_1 \right] = \Omega I_p L \int_0^1 \left[ N_{\beta_x} \right]^T \left[ N_{\beta_y} \right] d\xi \qquad \text{A23-24}$$

Where $\left[ N'_i \right] = \dfrac{\partial [N_i]}{\partial \xi}$ , with ($i = U, V, W, \beta_x , \beta_y , \phi$ )

**- Disk**

$$\left[ M_D^e \right] = \begin{bmatrix} \left[ I_m^D \right] & 0 & 0 & 0 & 0 & 0 \\ 0 & \left[ I_m^D \right] & 0 & 0 & 0 & 0 \\ 0 & 0 & \left[ I_m^D \right] & 0 & 0 & 0 \\ 0 & 0 & 0 & \left[ I_d^D \right] & 0 & 0 \\ 0 & 0 & 0 & 0 & \left[ I_d^D \right] & 0 \\ 0 & 0 & 0 & 0 & 0 & \left[ I_p^D \right] \end{bmatrix} , \qquad \text{A25}$$

$$\left[ G_D^e \right] = \begin{bmatrix} 0 & 0 & 0 & 0 & 0 & 0 \\ 0 & 0 & 0 & 0 & 0 & 0 \\ 0 & 0 & 0 & 0 & 0 & 0 \\ 0 & 0 & 0 & 0 & \Omega \left[ I_p^D \right] & 0 \\ 0 & 0 & 0 & -\Omega \left[ I_p^D \right]^T & 0 & 0 \\ 0 & 0 & 0 & 0 & 0 & 0 \end{bmatrix} \qquad \text{A26}$$

**- Bearings (Supports)**

$$\left[ K_P^e \right] = \begin{bmatrix} 0 & 0 & 0 & 0 & 0 & 0 \\ 0 & \left[ K_{yy} \right] & \left[ K_{yz} \right] & 0 & 0 & 0 \\ 0 & \left[ K_{zy} \right] & \left[ K_{zz} \right] & 0 & 0 & 0 \\ 0 & 0 & 0 & 0 & 0 & 0 \\ 0 & 0 & 0 & 0 & 0 & 0 \\ 0 & 0 & 0 & 0 & 0 & 0 \end{bmatrix} , \qquad \text{A27}$$

$$\left[ C_P^e \right] = \begin{bmatrix} 0 & 0 & 0 & 0 & 0 & 0 \\ 0 & \left[ C_{yy} \right] & \left[ C_{yz} \right] & 0 & 0 & 0 \\ 0 & \left[ C_{zy} \right] & \left[ C_{zz} \right] & 0 & 0 & 0 \\ 0 & 0 & 0 & 0 & 0 & 0 \\ 0 & 0 & 0 & 0 & 0 & 0 \\ 0 & 0 & 0 & 0 & 0 & 0 \end{bmatrix} \qquad \text{A28}$$

The elementary matrices of the system are

$$
\begin{cases}
\left[ M^e \right] = \left[ M_a^e \right] + \left[ M_D^e \right] \\
\left[ G^e \right] = \left[ G_a^e \right] + \left[ G_D^e \right] \\
\left[ K^e \right] = \left[ K_a^e \right] + \left[ K_P^e \right] \\
\left[ C_P^e \right]
\end{cases}
\qquad \text{A29}
$$

The various matrices (globally matrices) which assemble the elementary matrices, according to the boundary conditions as follows

$$
\begin{cases}
\left[ M \right] = \left[ M_a \right] + \left[ M_D \right] \\
\left[ G \right] = \left[ G_a \right] + \left[ G_D \right] \\
\left[ K \right] = \left[ K_a \right] + \left[ K_P \right] \\
\left[ C_P \right]
\end{cases}
\qquad \text{A30}
$$

The terms of the matrices are a function of the integrals: $J_{mn}^{\alpha\beta} = \int_0^1 f_m^\alpha\left(\xi\right) f_n^\beta\left(\xi\right) \; d\xi$ ;

$(m, n)$ indicate the number of the shape functions used, and $\left(\alpha,\beta\right)$ is the order of derivation.

## 7. References

Babuska, I. & Guo, B. (1986). The *h–p* version of the finite element method, Part I: the basic approximation results. *Computational Mechanics*, Vol. 1 , page numbers (21–41)

Bardell, N.S. (1996). An engineering application of the *h–p* version of the finite element method to the static analysis of a Euler–Bernoulli beam. Computers and Structures, Vol. 59, page numbers (195–211)

Bardell, N.S.; Dunsdon, J.M., & Langley, R.S. (1995). Free vibration analysis of thin rectangular laminated plate assemblies using the *h–p* version of the finite element method. *Composite Structures*, Vol. 32, page numbers (237–246)

Bert, C.W. & Kim, C.D. (1995a). Whirling of composite-material driveshafts including bending, twisting coupling and transverse shear deformation. *Journal of Vibration and Acoustics*, vol. 117, page numbers (17-21)

Bert, C.W. & Kim, C.D. (1995b). Dynamic instability of composite-material drive shaft subjected to fluctuating torque and/or rotational speed. *Dynamics and Stability of Systems*, Vol. 2, page numbers (125-147).

Bert, C.W. (1992). The effect of bending–twisting coupling on the critical speed of a driveshafts. *In: Proceedings. 6th Japan-US Conference on Composites Materials*, pp. 29-36, Orlando. FL. Technomic. Lancaster. PA

Boukhalfa, A. & Hadjoui, A. (2010). Free vibration analysis of an embarked rotating composite shaft using the *hp*- version of the FEM. *Latin American Journal of Solids and Structures*, Vol. 7, No. 2, page numbers (105-141)

Boukhalfa, A.; Hadjoui, A. & Hamza Cherif, S.M. (2008). Free vibration analysis of a rotating composite shaft using the *p*-version of the finite element method. *International Journal of Rotating Machinery*. Article ID 752062. 10 pages, Vol. 2008

Chang, M.Y.; Chang, M.Y. & Huang, J.H. (2004b). Vibration analysis of rotating composite shafts containing randomly oriented reinforcements. *Composite Structures*, Vol. 63, page numbers (21-32)

Chang, M.Y.; Chen, J.K. & Chang, C.Y. (2004a). A simple spinning laminated composite shaft model. *International Journal of Solids and Structures*, Vol. 41, page numbers (637–662)

Chatelet, E.; Lornage, D. & Jacquet-richardet, G. (2002). A three dimensional modeling of the dynamic behavior of composite rotors. *International Journal of Rotating Machinery*, Vol. 8, No. 3, page numbers (185-192)

Demkowicz, L.; Oden, J.T.; Rachowicz, W. & Hardy, O. (1989). Toward a universal *h–p* adaptive finite element strategy, Part I: constrained approximation and data structure. *Computational Methods in Applied Mechanics and Engineering*, Vol. 77, page numbers (79–112)

Dos Reis, H.L.M.; Goldman, R.B. & Verstrate, P.H. (1987). Thin walled laminated composite cylindrical tubes: Part III- Critical Speed Analysis. *Journal of Composites Technology and Research*, Vol. 9, page numbers (58–62)

Gupta, K. & Singh, S.E. (1996). Dynamics of composite rotors, *Proceedings of indo-us symposium on emerging trends in vibration and noise engineering*, pp. 59-70, New Delhi. India

Kim, C.D. & Bert, C.W. (1993). Critical speed analysis of laminated composite hollow drive shafts. *Composites Engineering*, Vol. 3, page numbers (633–643)

Singh, S.E. & Gupta, K. (1994b). Free damped flexural vibration analysis of composite cylindrical tubes using beam and shell theories. *Journal of Sound and Vibration*, Vol. 172, page numbers (171-190)

Singh, S.E. & Gupta, K. (1995). Experimental studies on composite shafts, *Proceedings of the International Conference on Advances in Mechanical Engineering*. , pp. 1205-1221, Bangalore. India

Singh, S.E. & Gupta, K. (1996). Composite shaft rotordynamic analysis using a layerwise theory. *Journal of Sound and Vibration*, Vol. 191, No. 5, page numbers (739–756)

Singh, S.P. & Gupta, K. (1994a). Dynamic analysis of composite rotors. *5th International Symposium on Rotating Machinery (ISROMAC-5)*. Also *International Journal of Rotating Machinery*, vol. 2, page numbers (179-186)

Singh, S.P. (1992). Some studies on dynamics of composite shafts. *Ph.D Thesis. Mechanical Engineering Department. IIT*, Delhi, India

Zinberg, H. & Symonds, M.F. (1970). The development of an advanced composite tail rotor driveshaft, *26th Annual Forum of The American Helicopter Society*, Washington. DC, June 1970
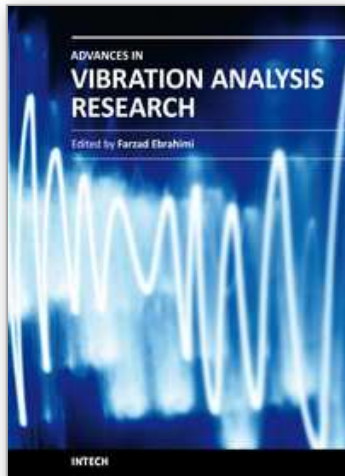
**Advances in Vibration Analysis Research**

Edited by Dr. Farzad Ebrahimi

Vibrations are extremely important in all areas of human activities, for all sciences, technologies and industrial applications. Sometimes these Vibrations are useful but other times they are undesirable. In any case, understanding and analysis of vibrations are crucial. This book reports on the state of the art research and development findings on this very broad matter through 22 original and innovative research studies exhibiting various investigation directions. The present book is a result of contributions of experts from international scientific community working in different aspects of vibration analysis. The text is addressed not only to researchers, but also to professional engineers, students and other experts in a variety of disciplines, both academic and industrial seeking to gain a better understanding of what has been done in the field recently, and what kind of open problems are in this area.

**How to reference**

In order to correctly reference this scholarly work, feel free to copy and paste the following:

# INTECH
open science | open minds